Mechanistic Study on Aerobic Oxidation of Amine over Intermetallic Pd₃Pb: Concerted Promotion Effects by Pb and Support Basicity

Shinya Furukawa,*,[†] Akifusa Suga,[‡] and Takayuki Komatsu*,[‡]

[†]Department of Chemistry and [‡]Department of Chemistry and Materials Science, Tokyo Institute of Technology, 2-12-1-E1-10 Ookayama, Meguro-ku, Tokyo 152-8551, Japan

Ⓢ *Supporting Information*

ABSTRACT: A mechanistic study on aerobic oxidation of amine to imine over Pd₃Pb/MO$_x$ (MO$_x$ = SiO₂, TiO₂, Al₂O₃, and MgO) intermetallic catalysts was performed to clarify the role of Pb and the support in enhancing catalytic activity. Results from X-ray absorption and photoelectron spectroscopies revealed that formation of the Pd₃Pb phase made Pd electron-rich compared to pure Pd, whereas the electronic states of Pd in Pd₃Pb/MO$_x$ were identical and independent of the nature of the support. Kinetic studies indicated that desorption of imine was promoted by Pb and that adsorption of amine was accelerated by basic sites on the support. Infrared temperature programmed desorption (IR-TPD) experiments demonstrated that desorption of imine was indeed promoted on Pd₃Pb compared to Pd. The support effect only appears on Pd₃Pb catalysts and not on pure Pd due to change in the rate-determining step from imine desorption to amine adsorption. The combination of Pb and the support basicity provides a unique and highly efficient bifunctional catalysis.

KEYWORDS: *Pd₃Pb, amine oxidation, intermetallic compound, concerted catalysis, mechanistic study*
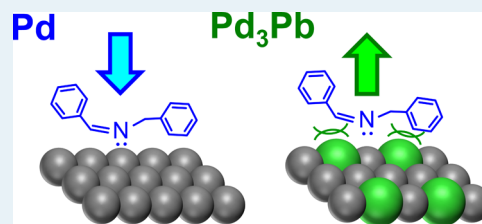
INTRODUCTION

Pd- or Pt-mediated oxidation is a very important chemical transformation in industrial chemistry, organic synthesis, and pharmaceuticals. To date, many effective catalytic oxidation systems have been reported. The principle one is aerobic oxidation of organic molecules such as alcohols,[1,2] amines,[3] and hydrocarbons.[4,5] In this field, development of Pd- or Pt-based bimetallic systems that are more effective than monometallic catalysts has been widely studied.[1,2] Among a series of second metal elements coupled with the noble metals, typical heavy elements such as Pb, Bi, Tl, and Te have been found to be most effective.[1,2] A number of rationales for the enhanced catalytic activity of these bimetallic systems have been reported: (1) so-called ensemble effects suppressing a side reaction yielding poisoning species (i.e., C−C cleavage),[6,7] (2) supply of adsorption sites for oxygen,[8−10] (3) complex formation between the second metal and the substrate,[11] (4) prevention of Pd corrosion,[2,12] (5) synergetic effects by the noble and second metals,[2,13] and (6) suppression of hydrogen sorption.[14] Recently, Baiker and co-workers employed in situ X-ray absorption fine structure (XAFS) and attenuated total reflection infrared (ATR-IR) techniques in aerobic oxidation of alcohols over a Pd−Bi catalyst, revealing that Bi inhibited side reactions and supplied oxygen to the catalyst surface.[15] They also used a similar technique to a Pt−Bi system and reported that Bi protected oxidation of Pt and blocked adsorption sites for solvent−Pt interaction.[16] Thus, informative insight has been provided by spectroscopic methods. However, the nature of this chemistry remains under discussion and is an attractive field for further investigation.

Very recently, we reported that supported Pd-based intermetallic compounds, such as Pd₃Pb and Pd₃Bi, showed much greater catalytic performances in aerobic oxidation of amine to imine than monometallic Pd.[17] A kinetic study implied that desorption of the product imine was promoted by formation of the intermetallic phase, enhancing the catalytic performance. This effect differs from those in the previously reported systems as mentioned above. Therefore, it would be a great impact in Pd-based oxidation chemistry to demonstrate and rationalize the unique effect of the second metal, Pb or Bi. However, we have obtained no obvious support including spectroscopic evidence, remaining the role of the second metal and the detailed reaction mechanism unclear. In addition to the effect of Pb, we also observed that basicity of the support strongly enhanced the catalytic activity of Pd₃Pb. In this context, a deep understanding of the reaction mechanism will also discover a unique concerted catalysis assisted by the second metal and the support.

In this study, detailed characterization of supported Pd₃Pb catalysts combined with kinetic studies in amine oxidation was performed to elucidate the reaction mechanism and the role of Pd₃Pb. A series of supported Pd₃Pb, Pd₃Pb/MO$_x$ (MO$_x$ = SiO₂, TiO₂, Al₂O₃, and MgO), were used also to clarify the effect of support on the catalytic performance. Herein, we propose not only a unique effect of Pb in Pd-based oxidation chemistry but

also a unique concerted catalytic system of Pd$_3$Pb and the support basicity.

EXPERIMENTAL SECTION

Materials. All chemical reagents except deuterated dibenzylamines were purchased or supplied: (NH$_4$)$_2$PdCl$_4$ (Aldrich, 97%), Pb(NO$_3$)$_2$ (Kanto, 99%), SiO$_2$ (Cariact G-6, Fuji Silysia Co., S_{BET} = 673 m^2 g^{-1}), TiO$_2$ (JRC-TIO-7, S_{BET} = 270 m^2 g^{-1}, anatase), Al$_2$O$_3$ (JRC-ALO-8, S_{BET} = 148 m^2 g^{-1}, γ + θ phase), MgO (JRC-MGO-4, S_{BET} = 28−38 m^2 g^{-1}), H$_2$ (Taiyo Nippon Sanso, 99.9999%), He (Taiyo Nippon Sanso, 99.9%), 5% O$_2$/ Ar (Taiyo Nippon Sanso), dibenzylamine (TCI, 97%), N-benzylidenebenzylamine (Wako, 96%), p-xylene (TCI, 99%), toluene (Kanto 99.5%), benzylamine-α,α-d2 (CDN Isotopes, 99.3 atom %D), benzyl bromide-α,α-d2 (CDN Isotopes, 98 atom %D), D$_2$O (Aldrich, 99.9 atom %D), dimethylformamide (TCI, 99.5%), Cs$_2$CO$_3$ (Kanto, 98%), Na$_2$SO$_4$ (Wako, 99%), BN (Wako, 99%).

Synthesis of Deuterated Dibenzylamines. (1) Dibenzylamine-$\alpha,\alpha,\alpha,\alpha$-$d$4 was synthesized by the following procedure. Benzyl bromide-α,α-d2 (5.5 mmol) in dimethylformamide (4 mL) was slowly added dropwise to a vigorously stirred mixture of benzylamine-α,α-d2 (5.5 mmol), Cs$_2$CO$_3$ (5.5 mmol), and dimethylformamide (6 mL) at 0 °C, which was subsequently stirred at 0 °C for 2 h. The reaction mixture was then filtered and the filtrate was concentrated by evaporation of dimethylformamide. A solution of 1 N NaOH (6 mL) and toluene (5 mL) was added to the concentrated residue, followed by extraction using toluene that was repeated four times. The organic layer was collected, dried by Na$_2$SO$_4$, concentrated, and distilled by Kugelrohr to afford 337 mg (31% yield) of colorless oil. ^{1}H NMR: (500 MHz, CD$_3$OD) δ 5.77 (8H, d), 5.70 (2H, m), 3.42 (1H, s).

(2) Dibenzylamine-N-d1 was synthesized by washing dibenzylamine (2.0 g) with D$_2$O (6 mL) three times, followed by extraction using toluene, evaporation, and Kugelrohr distillation.[18] A ^{1}H NMR spectrum indicated >90% deuterium content at the N-position by comparing of the integrated signal of the amino-proton with that of the benzylic.

Catalyst Preparation. In this study, Pd content was adjusted to 3.0 wt % for all Pd-containing catalysts. Pd/SiO$_2$ and Pd$_3$Pb/SiO$_2$ were prepared by a pore-filling impregnation. For Pd/SiO$_2$, aqueous solution of (NH$_4$)$_2$PdCl$_4$ was added to dried SiO$_2$ with the solution just filling the pores of the silica gel (1.64 mL ion-exchanged water per g-SiO$_2$). A mixed aqueous solution of (NH$_4$)$_2$PdCl$_4$ and Pb(NO$_3$)$_2$ with 3:1 molar ratio was used to obtain Pd$_3$Pb/SiO$_2$. The mixture was kept overnight at room temperature and then dried on a hot plate with stirring. The sample was reduced in a quartz tube with hydrogen flow (50 mL min^{-1}) at 400 °C for 1 h. Pb/SiO$_2$ (Pb: 3 wt %) was prepared by a similar procedure using Pb(NO$_3$)$_2$. Other supported Pd or Pd$_3$Pb catalysts (Pd/MO$_x$, Pd$_3$Pb/MO$_x$: MO$_x$ = TiO$_2$, Al$_2$O$_3$, and MgO) were prepared by a simple impregnation. It is difficult to perform pore-filling impregnation for these metal oxide supports due to the formation of a highly viscous slurry. A specific amount of aqueous solutions (at least for dissolving of salts) containing (NH$_4$)$_2$PdCl$_4$ alone or both (NH$_4$)$_2$PdCl$_4$ and Pb(NO$_3$)$_2$ with a 3:1 molar ratio were added dropwise to a vigorously stirred aqueous slurry of the oxide support (15 mL ion-exchanged water per g-support). After a stirring for 15 min in an air atmosphere, the slurry was completely dried on a hot plate and ground to a fine powder. The sample was then reduced in a quartz tube with hydrogen flow (50 mL min^{-1}) at a predetermined temperature for 1 h (Pd/TiO$_2$, 400 °C; Pd$_3$Pb/TiO$_2$, 450 °C; Pd/MgO, 500 °C; Pd/Al$_2$O$_3$, Pd$_3$Pb/Al$_2$O$_3$, and Pd$_3$Pb/MgO, 600 °C) to obtain nanoparticles of similar sizes. Unsupported bulk Pd$_3$Pb was prepared by arc melting of Pd and Pb beads with a 3:1 atomic ratio under an Ar atmosphere. The resulting ingot was crushed and ground into a fine powder.

Characterization. Dispersion of Pd was estimated by CO chemisorption under a dynamic condition using an assumption of 1:1 chemisorption to Pd atom. A certain amount of the catalyst (typically 100 mg) was placed in a quartz tube and reduced under flowing H$_2$ at 400 °C for 0.5 h. After the pretreatment, He was introduced at the same temperature for 0.5 h to remove hydrogen, followed by cooling to room temperature. A pulse of 5% CO/He was introduced into the reactor and the passed CO was quantified by a thermal conductivity detector downstream. This was repeated until the adsorption reached saturation. Powder X-ray diffraction (XRD) patterns of the prepared materials were recorded by a Rigaku RINT2400 using a Cu Kα X-ray source. The phase composition was calculated based on the intensity ratio Pd$_3$Pb 111 and Pd 111 diffractions and the atomic scattering factors[19] of Pd and Pb (see the Supporting Information for a detailed derivation). X-ray absorption experiments were carried out on a beamline BL01B1 at SPring-8 (Hyogo, Japan) with a ring energy of 8 GeV and a stored current from 60 to 100 mA. Prior to the measurement, the supported catalysts were pelletized, followed by reduction under a H$_2$ flow at 400 °C for 0.5 h. After the reduction pretreatment, the pellets were sealed into polyethylene bags under a dry Ar atmosphere without exposure to the air. Bulk Pd$_3$Pb powder was diluted with BN (boron nitride) and pelletized without any pretreatment. Pd−K edge (24.3 keV) and Pb−L$_{III}$ edge (13.0 keV) X-ray absorption fine structure (XAFS) spectra were recorded in transmission mode with quick scan. A fixed exit Si(111) double crystal monochromator with an energy resolution of ca. 0.3 eV in the X-ray absorption near edge structure (XANES) region was used. Higher harmonics were reduced by reflection on the two mirrors. For all spectra, a metallic Cu reference foil was used to provide an energy calibration for the monochromator. The XANES and extended XAFS (EXAFS) analyses were performed by Athena.[20] X-ray photoelectron spectra (XPS) of the intermetallic compounds were measured with an ULVAC PHI 5000 VersaProbe spectrometer. The catalyst was pressed into a pellet and placed into a quartz reactor, where it was reduced under flowing hydrogen (50 mL min^{-1}) at 400 °C for 0.5 h prior to measurement. Spectra were obtained with an Al Kα X-ray source, using C 1s as a reference for binding energy. Fourier-transformed infrared (FT-IR) spectra of the adsorbed imine were obtained with a JASCO FT/IR-430 spectrometer in transmission mode. A self-supporting wafer (20 mg cm^{-2}) of catalyst was placed in a quartz cell with CaF$_2$ windows and attached to a glass circulation system. The catalyst was reduced under flowing H$_2$ at 400 °C for 0.5 h, evacuated at the same temperature for 0.5 h, and cooled to room temperature. After the pretreatment, a spectrum was recorded as a baseline for the subsequent measurements. Degassed N-benzylidenebenzylamine (2.0 kPa) was introduced for 0.5 h and then evacuated. Temperature-programed desorption (TPD) of imine was subsequently carried out under evacuation at a ramping rate of 10 °C min^{-1}. A good linearity was obtained between the heating time and the actual temperature (Figure S1). All spectra were recorded at a 4 cm^{-1} resolution.

Catalytic Reaction. Catalyst (50 mg) was placed into a 50 mL three necked round-bottom flask equipped with a silicone ruber septum, a reflux condenser and a gas storage balloon (2 L) and was pretreated under H_2 stream (50 mL min^{-1}) at 400 °C for 0.5 h using a mantle heater. After pretreatment, dry Ar was passed into the flask to replace residual H_2 and the flask was cooled to room temperature. A reaction mixture containing solvent (p-xylene, 5 mL), amine (0.50 mmol), and an internal standard (biphenyl) was added into the flask through the septum. The atmosphere was then replaced with $O_2(5\%)$/Ar. Using the gas balloon provides an excess amount of O_2 toward amine (80 > O_2/amine molar ratio). The catalytic reaction was initiated by immersing the reaction apparatus into a preheated oil bath. The temperature of the oil bath was controlled to maintain the actual temperature of the reaction mixture at 110 °C. Products were quantified by flame-ionization detection gas chromatograph (FID-GC, Shimadzu GC14B equipped with a TC-17 capillary column) by using biphenyl as an internal standard. The turnover frequency was determined as the consumption rate of amine (mmol h^{-1}) per amount of exposed Pd (mmol) estimated by CO chemisorption. The initial consumption rates were typically obtained below 30% conversion. For the kinetic study, the O_2 content was adjusted by confluence of O_2 and Ar flows.

■ RESULTS AND DISCUSSION

Characterization of the Prepared Catalyst. The prepared Pd−Pb catalysts were characterized by XRD as shown in Figure 1. For all supports, apparent peaks
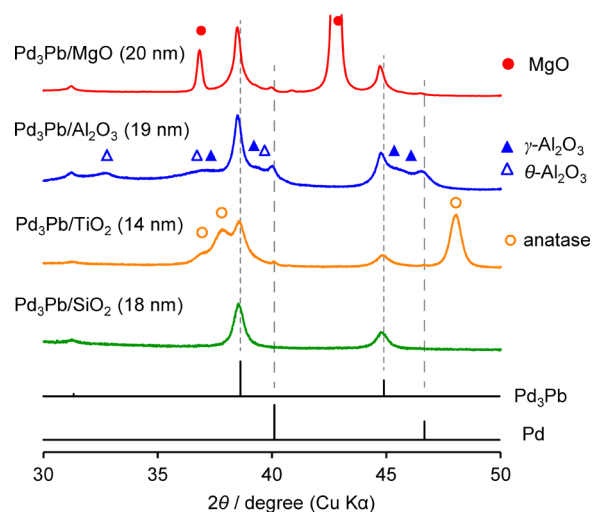
Figure 1. XRD patterns of supported Pd_3Pb catalysts. Numbers in parentheses indicate crystallite sizes estimated by Scherrer's equation.

corresponding to 111 and 200 diffractions of the Pd_3Pb phase were observed at 38.6° and 44.9°, respectively (PDF #04-002-9725). A small peak assigned to 110 diffraction of Pd_3Pb, which does not appear with an fcc structure due to distinction rule, was also observed at 31.3°. This indicates that the formed nanoparticles are truly the Pd_3Pb intermetallic phase (space group: $P\bar{m}3m$) but not $Pd_{0.75}Pb_{0.25}$ alloy (space group: $F\bar{m}3m$). The crystallite sizes of the supported Pd_3Pb nanoparticles were estimated by applying Scherrer's equation to the most intense 111 diffractions, which revealed similar sizes (14−20 nm, Table 1). The Pd_3Pb/SiO_2 catalyst showed no diffraction of monometallic Pd phase, suggesting the formation of Pd_3Pb in

Table 1. Analysis for Supported Pd_3Pb Catalysts[a]

	support			
	SiO_2	TiO_2	Al_2O_3	MgO
T_{red}/°C	400	450	600	600
D_{XRD}/nm	18	14	19	20
DP_{CO} (%)	2.3	2.0	2.7	4.0
Intensity Ratio (XRD)				
Pd_3Pb 111	1.00	0.95	0.83	0.95
Pd 111	0.00	0.05	0.17	0.05
Composition Fraction (XRD)				
Pd_3Pb	1.00	0.97	0.90	0.97
Pd	0.00	0.03	0.10	0.03
Composition Fraction (EXAFS)				
Pd_3Pb	0.97	0.97	0.87	0.94
Pd	0.03	0.03	0.13	0.06
r^2 ($k < 12$)	0.97	0.98	0.92	0.98

[a]T_{red}, reduction temperature; D_{XRD}, crystallite size estimated by Scherrer's equation; DP_{CO}, dispersion of Pd calculated by amount of chemisorbed CO assuming 1:1 adsorption.

a single phase. A similar result was also obtained for Pd_3Pb/TiO_2 or Pd_3Pb/MgO with only a tiny appearance of monometallic Pd. In the case of Pd_3Pb/Al_2O_3, small diffractions of monometallic Pd were observed in addition to the main peaks of the Pd_3Pb phase. The composition fractions of the Pd_3Pb and Pd phases were calculated based on the peak intensity (height) of the 111 diffractions (Table 1) and atomic scattering factors[19] of Pd and Pb (see the Supporting Information for the detailed derivation). The phase purity of Pd_3Pb on Al_2O_3 was estimated as 0.90. These results indicate that a small fraction of Pd did not participate in the formation of the intermetallic compound and remains in the monometallic phase. In general, the formation of an intermetallic compound tends to be inhibited by a support that strongly captures metal species, such as γ-Al_2O_3. Higher temperatures are typically required for successful formation of the intermetallic phase on such supports to increase atom mobility. Indeed, in the case of Pd_3Pb/Al_2O_3, an increase in the reduction temperature up to 800 °C enabled the formation of almost phase-pure Pd_3Pb (Figure S2). However, it should be noted that the increase in the reduction temperature also caused sintering of the intermetallic nanoparticles. We performed a similar XRD analysis also for the monometallic Pd catalysts. Diffractions corresponding to metallic Pd were observed (Figure S3), of which the estimated crystallite sizes were 20−27 nm (Table S1). The XRD analysis indicated that the desired intermetallic Pd_3Pb or monometallic Pd nanoparticles were successfully formed on several oxide supports. However, since small metallic clusters are XRD-unobservable (typically <2 nm), if any, their contribution to the phase purity cannot be evaluated by XRD analysis.

Therefore, we subsequently performed structural analysis of the supported catalysts using the XAFS technique. Figure 2a shows Pd−K edge EXAFS spectra of the supported Pb_3Pb catalysts and the reference samples. Authentic bulk Pd_3Pb showed an oscillation feature quite different from that of Pd foil, with a shorter period and smaller amplitude. According to the formula for EXAFS oscillation (eq 1), the shorter period is due to the longer Pd−Pd(Pb) distance (285 pm) of Pd_3Pb than that of Pd metal (275 pm).
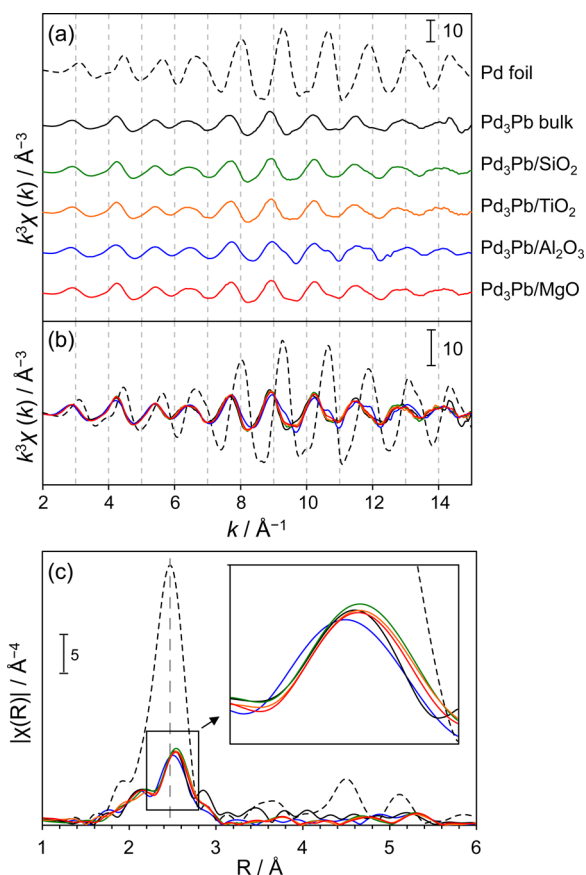
Figure 2. Pd−K edge EXAFS spectra of supported Pd$_3$Pb and reference compounds (a) with and (b) without offsets and (c) their Fourier transforms.

$$\chi(k) = S_0^2 \sum_j \frac{N_j F_j(k)\exp(-2k^2\sigma_j^2)}{kr_j^2}\sin(2kr_j + \varphi_j(k))$$

$$(1)$$

where, $\chi(k)$ is EXAFS oscillation, N_j is the number of scattering atoms, r_j is the distance to scattering atoms, $F_k(k)$ is the back scattering factor, σ_j is the Debye−Waller factor, $\varphi_j(k)$ is the phase shift, and S_0^2 is the many body effect. The smaller amplitude can be attributed to a much larger intrinsic Debye−Waller factor (thermal vibration) of Pb[21] than of Pd.[22] The difference in Pd−Pd(Pb) distance is represented more clearly in their Fourier transforms (Figure 2c). The EXASF oscillations and the Fourier transforms of the supported Pd$_3$Pb, except Pd$_3$Pb/Al$_2$O$_3$, were almost identical to that of bulk Pd$_3$Pb, which indicates two important points. One is the formation of Pd$_3$Pb intermetallic compound with high phase purity and the other is the absence of small Pd$_3$Pb or Pd clusters, because the presence of small clusters decreases the average coordination number and hence decreases the oscillation amplitude. According to the XRD analysis, a small fraction of monometallic Pd was contained in Pd$_3$Pb/Al$_2$O$_3$. In the corresponding EXAFS spectrum, only a small contribution of the monometallic Pd species was observed in the high k region ($k > 8$). The contribution of monometallic Pd was also confirmed in the Fourier transforms; this was indicated by a slightly shorter Pd−Pd(Pb) distance and smaller amplitude than those of other supported Pd$_3$Pb. The smaller amplitude can be attributed to a phase-cancellation by the two EXAFS

oscillations. The EXAFS oscillation of Pd$_3$Pb/Al$_2$O$_3$ was subsequently fitted by a linear combination of those of Pd$_3$Pb and Pd foils using a least-square method. A combination of 0.87 Pd$_3$Pb and 0.13 Pd gave the best fit with a 0.92 R^2 factor. Similar fitting was also performed for other supported Pd$_3$Pb catalysts (Table 1). The estimated values for Pd$_3$Pb fractions were consistent with the composition from XRD analysis. Pb−L$_{III}$ edge EXAFS spectra of the samples were also recorded as shown in Figure S4. The EXAFS oscillations of the supported Pd$_3$Pb catalysts were almost identical to that of bulk Pd$_3$Pb and quite different from the Pb foil. Thus, the information obtained by the EXAFS study agreed well with the results of XRD analysis and supported formation of the desired intermetallic particles with high phase purities.

Figure 3 shows the crystal structure of Pd$_3$Pb (a) in a single unit cell or (b) with a cuboctahedron shape and (c) the atomic
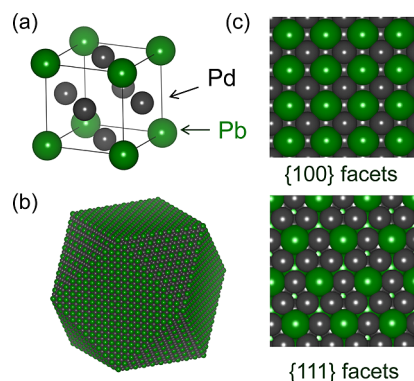
Figure 3. (a) Crystal structure of Pd$_3$Pb with single unit cell (PDF: #04-002-9725), (b) Pd$_3$Pb nanoparticle with cuboctahedron structure, and (c) its {100} and {111} facets.

arrangements on {100} and {111} facets. Pd$_3$Pb has an $L1_2$ type structure, i.e., the corner atoms in the unit cell of fcc Pd are replaced by Pb. Assuming a cuboctahedron structure, {100} and {111} facets are exposed in a 1:1.15 atomic ratio. When the particle size is 20 nm, based on this model the dispersion of Pd can be roughly estimated as 4.2%. This value agreed well with the dispersion measured by CO chemisorption for Pd$_3$Pb/MgO (4.0%) having a 20 nm crystallite size of Pd$_3$Pb (Table 1). Pd$_3$Pb/TiO$_2$ exhibited the lowest dispersion despite the size smaller than other samples. This may be due to so-called strong metal−support interaction (SMSI), which often results in coverage of metal particles with TiO$_2$ layer.[23,24] CO chemisorption was also carried out for the monometallic Pd catalysts. As summarized in Table S1, the obtained dispersions (3.9−7.9%) were close to those estimated by the cuboctahedron model (4.6−6.0%). Thus, for both Pd$_3$Pb and monometallic Pd catalysts, good agreements were obtained between the measured and estimated dispersions. This indicates the validity of the cuboctahedron model and the absence of small metal clusters, which will significantly increase the dispersion of Pd.

We subsequently investigated the electronic states of the prepared catalysts by XANES and XPS. Figure 4 shows Pd−K edge XANES spectra of the supported Pd$_3$Pb catalysts and reference samples. For bulk Pd$_3$Pb, the energy of absorption edge (E_0) and the height of the white line (H_w) corresponding to the 1s → 5p transition were lower than those of Pd foil, indicating the electron-richness of Pd atoms in Pd$_3$Pb compared to those in monometallic Pd. The supported
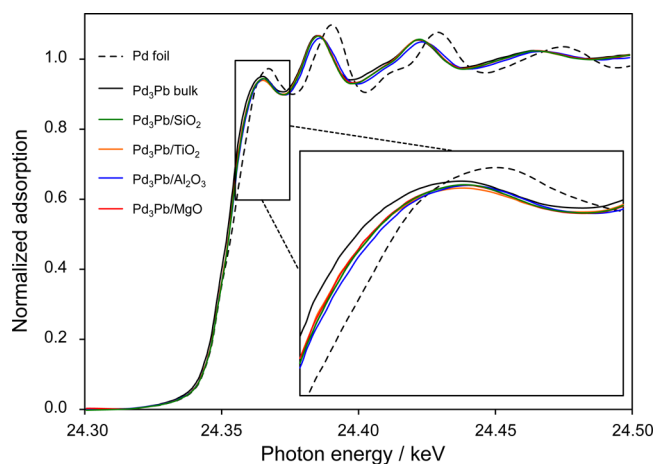
Figure 4. Pd−K edge XANES spectra of supported Pd₃Pb and reference compounds.

Pd₃Pb catalysts showed spectral features similar to that of bulk Pd₃Pb. A small deviation of E_0 was observed between the bulk and supported samples, which may be attributed to the difference in the style, that is, the bulk or supported particles. The spectral features of the supported catalysts were almost identical with each other. Only a tiny difference in E_0 (closer to that of Pd foil) was observed for the Al₂O₃-supported catalyst. Based on the structural analyses mentioned above, this could be due to the presence of a small amount of monometallic Pd. These results suggest that the electronic state of Pd in Pd₃Pb is minimally dependent on the nature of the support. Figure 5
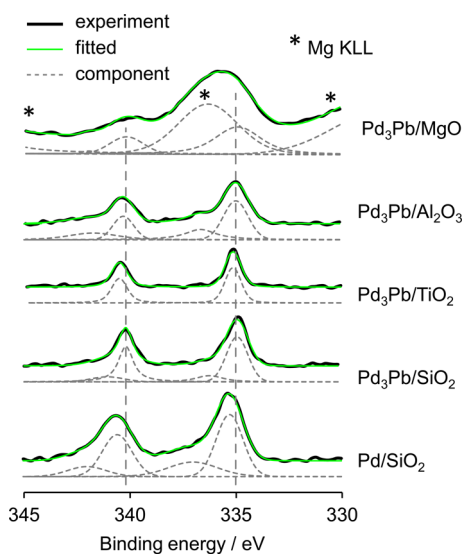
Figure 5. Pd 3d XPS of Pd/SiO₂ and supported Pd₃Pb catalysts.

shows Pd 3d XPS of Pd/SiO₂ and the supported Pd₃Pb catalysts. Pd/SiO₂ exhibited 3d emission peaks at 335.3 ($3d_{5/2}$) and 340.6 ($3d_{3/2}$) eV that were consistent with the reported values of metallic Pd supported on SiO₂.[25] A small fraction of the cationic species was also observed. The peak positions of metallic Pd for Pd₃Pb/SiO₂ were lower in energy than those of Pd/SiO₂. This result indicates that Pd atoms at the surface of Pd₃Pb supported on SiO₂ are electron-rich than those of Pd/SiO₂, which is consistent with the result of XANES. Pd₃Pb/TiO₂ and Pd₃Pb/Al₂O₃ showed emission peaks with positions

similar to those of Pd₃Pb/SiO₂. In the case of Pd₃Pb/MgO, intense peaks owing to Mg KLL Auger processes[26] were also observed with an appearance of the Pd 3d emissions. Peak deconvolution revealed that the peak positions for the Pd 3d emissions were almost identical to those of other supported Pd₃Pb samples. An XPS analysis of Pb 4f region was also carried out. All the supported Pd₃Pb samples showed Pb 4f emission peaks at around 136.6 ($4f_{7/2}$) and 141.4 ($4f_{5/2}$) eV, corresponding to metallic Pb (Figure S5).[27−29] The presence of cationic lead assignable to PbO₂[27−30] was also detected, particularly for Pd₃Pb/Al₂O₃. This is probably due to the presence of residual Pb, which did not participate in the intermetallic formation as mentioned above, being in the oxide phase. Minimal differences in the peak positions of PbO₂ were observed among the samples. On the basis of the electronic analyses by XANES and XPS, we concluded that the electronic states of the supported Pd₃Pb particles were almost identical and independent of the nature of the support.

Aerobic oxidation of dibenzylamine into *N*-benzylidenebenzylamine was carried out over the supported Pd₃Pb and Pd catalysts. Figure 6 shows the time course of amine conversion
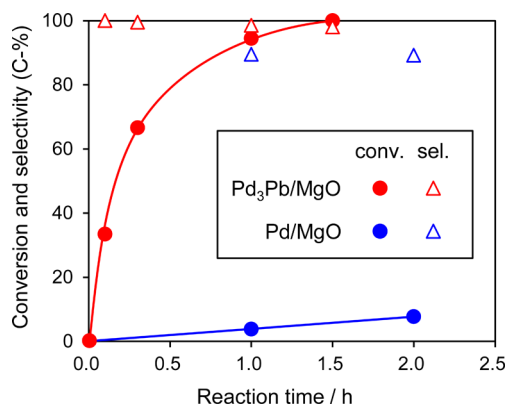
Figure 6. Time course of dibenzylamine conversion and *N*-benzylidenebenzylamine selectivity in aerobic oxidation of dibenzylamine over Pd₃Pb/MgO and Pd/MgO.

and imine selectivity when Pd₃Pb/MgO or Pd/MgO was used as a catalyst. Pd/MgO showed a very low conversion (8% at 2 h), whereas Pd₃Pb/MgO exhibited remarkably high catalytic activity (100% at 1.5 h). For Pd/MgO, small amounts of benzaldehyde and benzylamine were formed as fragmented byproducts, which resulted in 89 C% imine selectivity. The formation of these byproducts was inhibited over Pd₃Pb/MgO, affording an excellent selectivity (98 C% at 100% conversion). The turnover number (TON) and turnover frequency (TOF/ h^{-1}) were calculated as the yield (mmol) and formation rate (mmol h^{-1}) of imine per number of exposed Pd atoms (mmol), respectively. Pd/MgO gave 16 h^{-1} of initial TOF and 32 of TON after 2 h of reaction, indicating that the reaction catalytically proceeded in spite of the very low conversion. Much higher initial TOF (2990 h^{-1}) and TON (892, 1.5 h) were obtained using Pd₃Pb/MgO than Pd/MgO. In a similar fashion, the initial TOF values were estimated for other Pd₃Pb and Pd catalysts. For Pd₃Pb catalysts, the order of the obtained TOF values was 470 (Pd₃Pb/SiO₂) < 1710 (Pd₃Pb/TiO₂) < 2120 (Pd₃Pb/Al₂O₃) < 2990 (Pd₃Pb/MgO). Since the electronic states of Pd in these catalysts are almost identical as mentioned above, it is likely that the nature of the support itself contributed to the reaction outcome. Figure 7 shows the
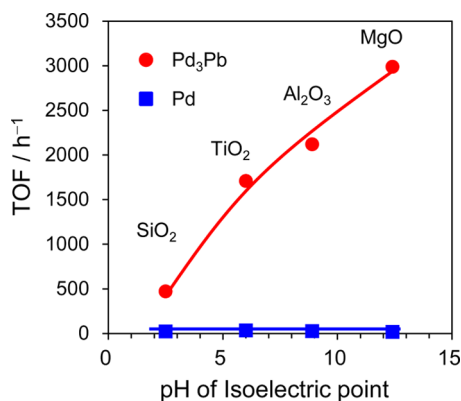
Figure 7. Relation between TOF in dibenzylamine oxidation and pH of isoelectric point of catalyst support.

relationship between the obtained TOF and the pH of support's isoelectric point, as a scale of its basicity. An obvious positive correlation with support basicity was observed for Pd₃Pb catalysts. In the previous study, we observed a similar relationship; however, the catalytic activity increased exponentially with increase in the support basicity, where the Pd dispersion had not been considered.[17] The true relationship was thus obtained by taking the dispersion into account. For monometallic Pd catalysts, in contrast, all TOF values were similar, remaining small and independent of the support basicity: 21 (Pd/SiO₂), 32 (Pd/TiO₂), 24 (Pd/Al₂O₃), and 16 (Pd/MgO). Thus, the positive effect of support basicity was observed only with Pd₃Pb catalysts and not monometallic Pd catalysts. Emphasis should be placed on the fact that the TOF was ca. 190 times higher using Pd₃Pb/MgO compared to Pd/MgO. Even for SiO₂-supported catalysts, TOF was ca. 20 times higher for Pd₃Pb/SiO₂ than for Pd/SiO₂.

Kinetic studies were subsequently performed to elucidate the reaction mechanism. We have observed above two prominent contributions to the catalytic activity, i.e., the Pd₃Pb phase and the support basicity. It is better to consider these contributions individually. To clarify the role of the Pd₃Pb phase without any involvement of the support basicity, we initially chose silica-supported catalysts (Pd₃Pb/SiO₂ and Pd/SiO₂) as the targets in the kinetic study. Figure 8 shows the dependence of the reaction rates on (a) amine concentration, [S], and (b) the partial pressure of O₂, P_{O_2}. Pd₃Pb/SiO₂ displayed a first-order relationship with [S] and a zero-order dependence on P_{O_2}, suggesting that adsorption of amine is the rate-determining step. In contrast, for Pd/SiO₂, the reaction orders with [S] and P_{O_2} were both close to zero, indicating that adsorption of amine and the O₂-involved step are not rate-determining. With the increase in P_{O_2} over the standard condition, the reaction order became negative in the case of Pd₃Pb. This result suggests that competitive adsorption of amine and O₂ occurs in this pressure region. In this context, saturation coverage of O₂ around the standard condition is not likely despite the zero-order dependence. To further understand the reaction mechanism, we subsequently performed a kinetic isotope study using deuterized amines as described in Scheme 1. For Pd₃Pb/SiO₂, deuteration at the amino position of dibenzylamine (dibenzylamine-N-d1) showed a positive kinetic isotope effect (KIE, k_H/k_D = 2.2, Scheme 1a). Combined with the first-order dependence on [S], it appears that dissociative adsorption of dibenzylamine (N−H scission) is the rate-determining step for Pd₃Pb/SiO₂. A similar KIE value (k_H/k_D = 2.3) was obtained
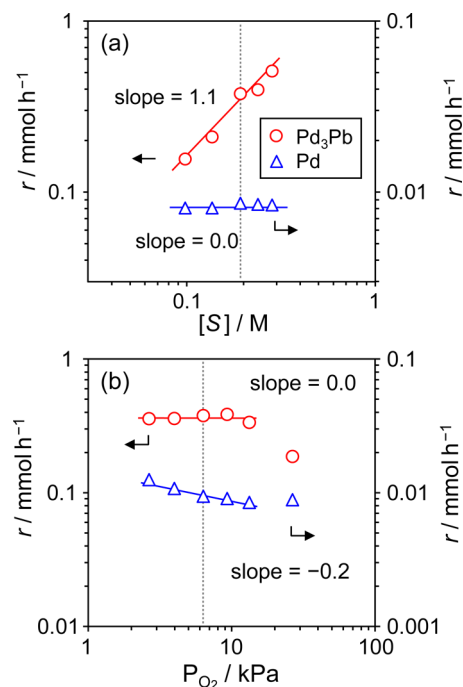
Figure 8. Reaction rates (r) over Pd₃Pb/SiO₂ and Pd/SiO₂ as functions of (a) amine concentration ([S]) and (b) oxygen pressure (P_{O_2}). The standard conditions are designated as dotted lines.

Scheme 1. Kinetic Isotope Effects for (a) Amino and (b) Benzylic Positions of Dibenzylamine
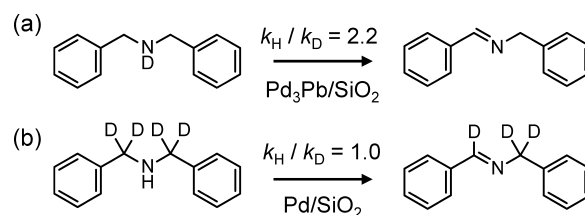
when Pd₃Pb/MgO was used as a catalyst (data not shown), indicating that dissociative adsorption of amine remained rate-determining even for Pd₃Pb/MgO. In the case of Pd/SiO₂, we focused on C−H activation at the α position of dibenzylamine, which is mandatory for imine formation. For this purpose, dibenzylamine-$\alpha,\alpha,\alpha,\alpha$-d4, of which all α hydrogen atoms were deuterized, was used as a substrate. However, no KIE was observed (k_H/k_D = 1.0, Scheme 1b), revealing that the C−H activation step is similarly not rate-determining for Pd/SiO₂. Pd/MgO as a catalyst gave a similar result (k_H/k_D = 0.9), suggesting no kinetic difference between Pd/MgO and Pd/SiO₂. A similar kinetic study using dibenzylamine-N-d1 was also performed for Pd/SiO₂, revealing a KIE value close to unity (k_H/k_D = 1.3). This result indicates that dissociative adsorption of dibenzylamine is not the rate-determining step for Pd/SiO₂, which is consistent with the zero-order dependence on amine concentration mentioned above.

On the basis of the obtained results, we propose a plausible reaction mechanism shown in Scheme 2a. First, dissociative adsorption of amine occurs over Pd atoms. This process results in the formation of Pd−H and Pd−amide species (1). C−H activation at the α position against N, corresponding to the β position against Pd, takes place to form imine (2), which is so-called β-H elimination. The formed imine is then desorbed as a

Scheme 2. (a) Reaction Mechanism of Amine Oxidation over Pd₃Pb/SiO₂ and (b) Deprotonation by a Basic Site on TiO₂, Al₂O₃, or MgO[17]
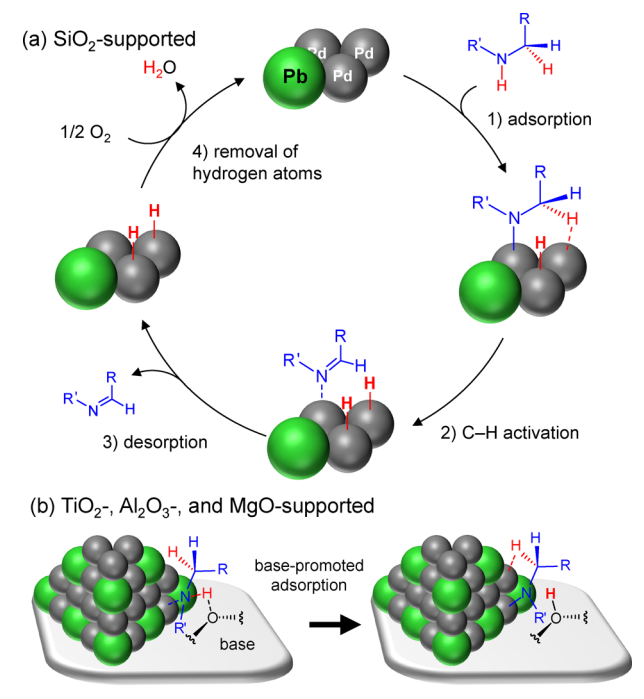
product (3). Finally, the eliminated hydrogen atoms are consumed by O_2 to form H_2O (4). In the case of Pd/SiO_2, steps 1, 2, and 4 are not rate-determining as indicated above. Therefore, it can be said that the desorption of imine (3) is the rate-determining step for Pd/SiO_2. This implies a strong adsorption capability of imine to Pd, most likely due to a

contribution of π back-bonding interaction, in addition to coordination with the lone pair. In the literature, a similar situation can be observed in alcohol oxidation using Pd catalysts; the presence of heteroatoms, such as N and S, in alcoholic substrates fatally deactivates the catalysis probably by poisoning Pd sites.[31] In contrast, for Pd_3Pb/SiO_2, the situation is drastically altered; the rate-determining step is shifted to adsorption (1). Considering the enhanced catalytic activity, this shift can be attributed to an acceleration of imine desorption. Thus, the role of the Pd_3Pb phase or Pb itself was suggested as a desorption promoter. In addition to the positive role of the intermetallic phase, we observed another effect by involving the support basicity. For Pd_3Pb catalysts, it is likely that the basicity contributes to adsorption of amine as this step is rate-determining. A possible interpretation is that deprotonation from amine by neighboring basic sites on the support promotes the formation of amide species (Scheme 2b). The stronger the basicity, the more promoted the deprotonation. Indeed, some of us recently reported that the dissociative adsorption of amine took place on a metal oxide surface to form metal-amide and a hydroxyl group.[32] This has been demonstrated by an FT-IR study using benzylamine-N-d2, which reported the formation of amide species and surface O−D bonds. In the case of TiO_2-, Al_2O_3-, and MgO-supported Pd_3Pb catalysts, in this context, metal−support interfaces seem to be the most effective reaction sites. In contrast, for monometallic Pd catalysts, as the reaction rate is limited by desorption, such a promotion effect in adsorption was not reflected in the catalytic activity. Thus, in this catalytic system, a combination of desorption and adsorption promoters afforded a remarkable enhancement in the catalytic activity.

It is also important to consider the contribution of oxygen to the oxidation state of surface Pd and Pb. When we performed the amine oxidation with Pd_3Pb/SiO_2 without H_2 reduction
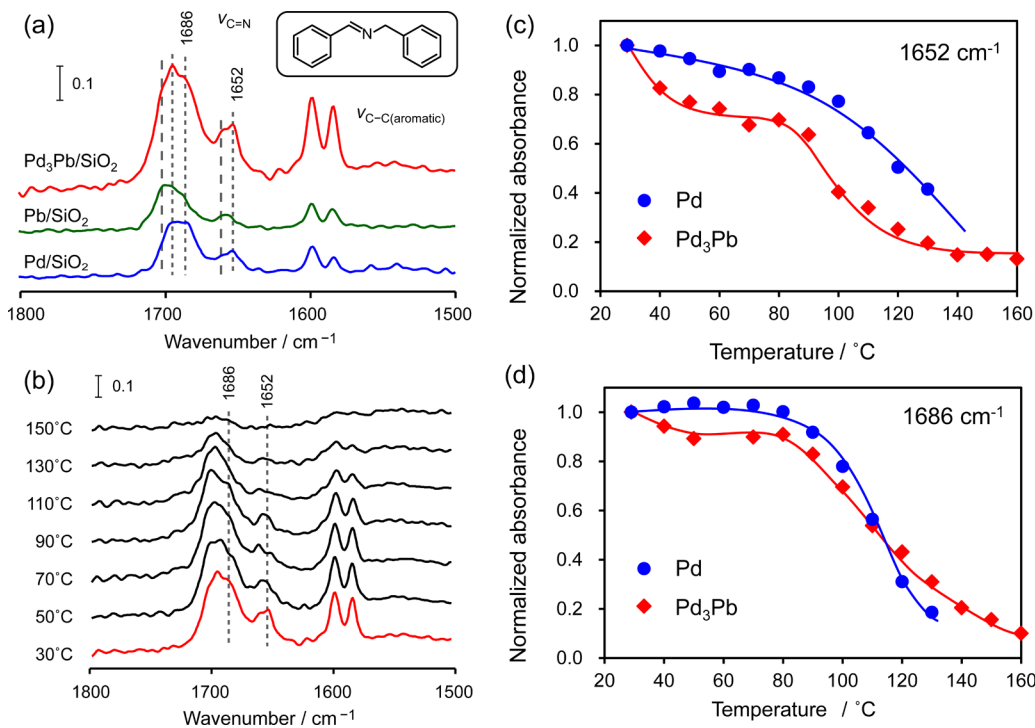
Figure 9. (a) FT-IR spectra of N-benzylidenebenzylamine adsorbed on Pd_3Pb/SiO_2, Pb/SiO_2, and Pd/SiO_2. (b) Change in FT-IR spectra of imine adsorbed on Pd_3Pb/SiO_2 during heating at 10 °C min⁻¹ under evacuation. TPD profiles of imine at (c) 1652 and (d) 1686 cm⁻¹.

pretreatment, the catalytic activity drastically dropped compared to that with the treatment (data not shown). Therefore, it seems to be important for the catalysis that Pd and Pb are in metallic state. A recent in situ XAFS study for alcohol oxidation over Pd–Bi catalysts revealed that both Pd and Bi kept metallic states during the reaction in the presence of 1 atm O_2 and that after the complete consumption of alcohol Bi was oxidized into Bi^{3+} state.[15] It appears that alcohol prevents the oxidation of metallic species probably because O_2 reacts preferentially with the eliminated hydrogen. A similar effect may work in our system, hence prevent the oxidation of Pd and Pb.

To obtain evidence of the promoted desorption on Pd_3Pb, we performed TPD of imine monitored by FT-IR. Figure 9a shows the FT-IR spectra of *N*-benzylidenebenzylamine, the reaction product, chemisorbed on Pd_3Pb/SiO_2, Pb/SiO_2, and Pd/SiO_2. Peaks assigned to C=N stretching vibration appeared intensely in the region of 1650−1700 cm^{-1}. A slight difference in the peak position was observed between Pd/SiO_2 (1652, 1686, and 1695 cm^{-1}) and Pb/SiO_2 (1659, 1695, and 1702 cm^{-1}), whereas Pd_3Pb/SiO_2 exhibited both features. These assignments were summarized in Table S2. Figure 9b shows the spectral changes for Pd_3Pb/SiO_2 during heating at 10 °C min^{-1} under vacuum. A decrease in the peak intensities was observed with an increase in temperature, corresponding to desorption of imine. Similar results were also obtained for Pd/SiO_2 and Pb/SiO_2 (Figure S6). To construct a TPD profile for Pd sites, the changes in peak intensity at 1652 cm^{-1} (Figure 9c) and 1686 cm^{-1} (Figure 9d) were plotted with respect to temperature for Pd_3Pb/SiO_2 and Pd/SiO_2. In the case of Pd/SiO_2, desorption began at ca. 80 °C. In contrast, for Pd_3Pb/SiO_2, desorption occurred near room temperature, providing strong evidence for promoted desorption on Pd sites of Pd_3Pb/SiO_2. In the TPD profiles of Pd_3Pb/SiO_2, desorption seems to proceed via a stepwise fashion, that is, 25−80 and 80−160 °C. This may be due to overlapping of the desorption from Pb sites as a shoulder. It is clearly evident in Figure 9b that the significant decrease at 1704 or 1694 cm^{-1} occurred at a much higher temperature than that at 1686 cm^{-1}. Therefore, the first decrease (25−80 °C) in the TPD profile can be assigned to desorption from Pd sites and the second (80−160 °C) from Pb sites. A similar situation is observed in Figure S6; desorption from Pd/SiO_2 completed at 130 °C, whereas that from Pb/SiO_2 at 150 °C, indicating that desorption from the Pb sites is more endothermic than from Pd sites. These results suggest that Pb atoms themselves do not act as effective desorption sites but diminish the imine-holding capability of Pd sites.

Finally, we discuss the essential role of Pb, regarding why desorption is promoted. As mentioned above, the electronic state of Pd was modified to be electron-rich by the formation of the Pd_3Pb phase. Because imine is coordinated to Pd with a lone pair as a base, an electron-enriched Pd site seems to facilitate desorption of imine. In this context, such an electronic effect looks plausible to explain the enhanced catalytic activity. However, we should also consider our previous results of a series of Pd-based intermetallic compounds in terms of the electronic effect. For example, $Pd_{13}Pb_9$ and Pd_3Bi also showed good catalytic performances comparable to Pd_3Pb.[17] However, we previously reported that Pd atoms consisting of $Pd_{13}Pb_9$ were electron-deficient compared to monometallic Pd.[33] Moreover, although it has been reported by some researchers that Pd atoms in PdGa[34,35] and PdZn[36−38] were negatively charged, these compounds exhibited much lower catalytic performances than Pd_3Pb (comparable to monometallic Pd).[17]

Therefore, the specifically high catalytic activities of Pd_3Pb, $Pd_{13}Pb_9$, and Pd_3Bi cannot be explained by the electronic effect. A possible interpretation alternative to the electronic effect is a geometric one. Since Pb and Bi atoms have considerably larger metallic radii than Pd (Pb, 1.75 Å; Bi, 1.70 Å; Pd, 1.37 Å),[39] steric repulsion at the Pd site should be greater than that of monometallic Pd due to the presence of the neighboring Pb or Bi atom. This situation can be observed with Pd_3Pb (111) and Pd_3Pb (100) surfaces as shown in Figure 3. Such a steric hindrance seems to significantly weaken adsorption of imine, promoting desorption. Furthermore, this interpretation is consistent with the result of IR-TPD measurement, which showed the milder imine-capturing capability of Pd.

CONCLUSION

In this study, a mechanistic study based on kinetic and spectroscopic approaches revealed the detailed catalysis of aerobic amine oxidation over intermetallic Pd_3Pb catalysts and the role of Pb in enhancing the catalytic activity. Oxidative dehydrogenation of amine to imine occurs via N−H scission, α-C−H activation, desorption of imine, and removal of hydrogen by O_2. For a monometallic Pd catalyst, strong coordination of imine to Pd causes imine desorption to be rate-determining. In contrast, for Pd_3Pb, desorption of imine is promoted by Pb, which results in the shift of the rate-determining step to adsorption of amine. Adsorption of amine is accelerated by deprotonation by the basic site on the support, which further enhances the catalytic activity. However, in the case of monometallic Pd, because the reaction rate is limited by desorption of imine, such a promotion effect of the basicity is not reflected in the catalytic activity. Thus, in the oxidation of amine over supported Pd-based intermetallic catalysts, a combination of the effects of the second metal and the support basicity constitutes a well-concerted bifunctional catalysis. The obtained insights in the present study have significant implications for Pd-based oxidation chemistry.

ASSOCIATED CONTENT

Supporting Information

The following file is available free of charge on the ACS Publications website at DOI: 10.1021/cs501695m.

> Derivation of phase composition from peak intensity in XRD pattern, Tables S1 and S2, and Figures S1–S6 (PDF)

AUTHOR INFORMATION

Corresponding Authors
*E-mail: furukawa.s.af@m.titech.ac.jp. Tel.: +81-3-5734-2602. Fax: +81-3-5734-2758 (S.F.).
*E-mail: komatsu.t.ad@m.titech.ac.jp. Tel.: +81-3-5734-3532. Fax: +81-3-5734-2758 (T.K.).

Notes
The authors declare no competing financial interest.

ACKNOWLEDGMENTS

■ REFERENCES

(1) Mallat, T.; Baiker, A. *Chem. Rev.* **2004**, *104*, 3037−3058.

(2) Mallat, T.; Baiker, A. *Catal. Today* **1994**, *19*, 247−283.

(3) Wang, J. R.; Fu, Y.; Zhang, B. B.; Cui, X.; Liu, L.; Guo, Q. X. *Tetrahedron Lett.* **2006**, *47*, 8293−8297.

(4) Choudhary, T. V.; Banerjee, S.; Choudhary, V. R. *Appl. Catal. A: Gen.* **2002**, *234*, 1−23.

(5) Lin, M. R.; Hogan, T.; Sen, A. *J. Am. Chem. Soc.* **1997**, *119*, 6048−6053.

(6) Herrero, E.; Fernandezvega, A.; Feliu, J. M.; Aldaz, A. *J. Electroanal. Chem.* **1993**, *350*, 73−88.

(7) Mallat, T.; Baiker, A.; Patscheider, J. *Appl. Catal.* **1991**, *79*, 59−75.

(8) Ocon, P.; Beden, B.; Lamy, C. *Electrochim. Acta* **1987**, *32*, 1095−1101.

(9) Mallat, T.; Bodnar, Z.; Baiker, A.; Greis, O.; Strubig, H.; Reller, A. *J. Catal.* **1993**, *142*, 237−253.

(10) Furuya, N.; Motoo, S. *J. Electroanal. Chem.* **1979**, *98*, 189−194.

(11) Smits, P. C. C.; Kuster, B. F. M.; Vanderwiele, K.; Vanderbaan, H. S. *Appl. Catal.* **1987**, *33*, 83−96.

(12) Tsujino, T.; Ohigashi, S.; Sugiyama, S.; Kawashiro, K.; Hayashi, H. *J. Mol. Catal.* **1992**, *71*, 25−35.

(13) Fiege, H.; Wedemeyer, K. *Angew. Chem., Int. Ed.* **1981**, *20*, 783−784.

(14) Parsons, R.; Vandernoot, T. *J. Electroanal. Chem.* **1988**, *257*, 9−45.

(15) Mondelli, C.; Ferri, D.; Grunwaldt, J. D.; Krumeich, F.; Mangold, S.; Psaro, R.; Baiker, A. *J. Catal.* **2007**, *252*, 77−87.

(16) Mondelli, C.; Grunwaldt, J. D.; Ferri, D.; Baiker, A. *Phys. Chem. Chem. Phys.* **2010**, *12*, 5307−5316.

(17) Furukawa, S.; Suga, A.; Komatsu, T. *Chem. Commun.* **2014**, *50*, 3277−3280.

(18) Smith, J. K.; Bergbreiter, D. E.; Newcomb, M. *J. Org. Chem.* **1985**, *50*, 4549−4553.

(19) Brown, P. J.; Fox, A. G.; Maslen, E. N.; O'Keefec, A.; Willisd, B. T. M. In *International Tables for Crystallography*; Prince, E., Ed.; Wiley-VCH: Weinheim, 2006; Vol. C, p 544−590.

(20) Ravel, B.; Newville, M. *J. Synchrotron Radiat.* **2005**, *12*, 537−541.

(21) Yu, Y. H.; Tyliszczak, T.; Hitchcock, A. P. *J. Phys. Chem. Solids* **1990**, *51*, 445−451.

(22) Kochubey, D. I.; Pavlova, S. N.; Novgorodov, B. N.; Kryukova, G. N.; Sadykov, V. A. *J. Catal.* **1996**, *161*, 500−506.

(23) Tauster, S. J.; Fung, S. C.; Baker, R. T. K.; Horsley, J. A. *Science* **1981**, *211*, 1121−1125.

(24) Tauster, S. J.; Fung, S. C.; Garten, R. L. *J. Am. Chem. Soc.* **1978**, *100*, 170−175.

(25) Huang, L.; Wang, Z.; Ang, T. P.; Tan, J.; Wong, P. K. *Catal. Lett.* **2006**, *112*, 219−225.

(26) Claus, P.; Berndt, H.; Mohr, C.; Radnik, J.; Shin, E. J.; Keane, M. A. *J. Catal.* **2000**, *192*, 88−97.

(27) Hirano, T.; Ozawa, Y.; Sekido, T.; Ogino, T.; Miyao, T.; Naito, S. *Appl. Catal. A: Gen.* **2007**, *320*, 91−97.

(28) Hirano, T.; Kazahaya, Y.; Nakamura, A.; Miyao, T.; Naito, S. *Catal. Lett.* **2007**, *117*, 73−78.

(29) Abdel−Samad, H.; Watson, P. R. *Appl. Surf. Sci.* **1998**, *136*, 46−54.

(30) Evarestov, R. A.; Veryazov, V. A. *Phys. Stat. Sol. B* **1991**, *165*, 411−418.

(31) Kakiuchi, N.; Maeda, Y.; Nishimura, T.; Uemura, S. *J. Org. Chem.* **2001**, *66*, 6620−6625.

(32) Furukawa, S.; Ohno, Y.; Shishido, T.; Teramura, K.; Tanaka, T. *J. Phys. Chem. C* **2013**, *117*, 442−450.

(33) Furukawa, S.; Yoshida, Y.; Komatsu, T. *Acs Catal.* **2014**, *4*, 1441−1450.

(34) Kovnir, K.; Armbruster, M.; Teschner, D.; Venkov, T. V.; Szentmiklosi, L.; Jentoft, F. C.; Knop-Gericke, A.; Grin, Y.; Schlogl, R. *Surf. Sci.* **2009**, *603*, 1784−1792.

(35) Kovnir, K.; Armbruster, M.; Teschner, D.; Venkov, T. V.; Jentoft, F. C.; Knop-Gericke, A.; Grin, Y.; Schlogl, R. *Sci. Technol. Adv. Mater.* **2007**, *8*, 420−427.

(36) Armbruster, M.; Behrens, M.; Fottinger, K.; Friedrich, M.; Gaudry, E.; Matam, S. K.; Sharma, H. R. *Catal. Rev.* **2013**, *55*, 289−367.

(37) Friedrich, M.; Teschner, D.; Knop-Gericke, A.; Armbruster, M. *J. Catal.* **2012**, *285*, 41−47.

(38) Iwasa, N.; Takezawa, N. *Top. Catal.* **2003**, *22*, 215−224.

(39) Pauling, L. *J. Am. Chem. Soc.* **1947**, *69*, 542−553.